Atmospheric Environment 43 (2009) 4327–4338

Contents lists available at ScienceDirect

Atmospheric Environment

journal homepage: www.elsevier.com/locate/atmosenv

# Evaluating inter-continental transport of fine aerosols: (1) Methodology, global aerosol distribution and optical depth

Junfeng Liu [a,*], Denise L. Mauzerall [a,**], Larry W. Horowitz [b], Paul Ginoux [b], Arlene M. Fiore [b]

[a] Woodrow Wilson School, Princeton University, Princeton, NJ 08544, USA
[b] Geophysical Fluid Dynamics Laboratory, Princeton, NJ 08540, USA

ARTICLE INFO

*Article history:*
Received 14 November 2008
Received in revised form
28 March 2009
Accepted 31 March 2009

*Keywords:*
Inter-continental transport
Source-receptor relationships
Aerosols
Air quality
Optical depth

ABSTRACT

Our objectives are to evaluate inter-continental source-receptor relationships for fine aerosols and to identify the regions whose emissions have dominant influence on receptor continents. We simulate sulfate, black carbon (BC), organic carbon (OC), and mineral dust aerosols using a global coupled chemistry-aerosol model (MOZART-2) driven with NCEP/NCAR reanalysis meteorology for 1997–2003 and emissions approximately representing year 2000. The concentrations of simulated aerosol species in general agree within a factor of 2 with observations, except that the model tends to overestimate sulfate over Europe in summer, underestimate BC and OC over the western and southeastern (SE) U.S. and Europe, and underestimate dust over the SE U.S. By tagging emissions from ten continental regions, we quantify the contribution of each region's emissions on surface aerosol concentrations (relevant for air quality) and aerosol optical depth (AOD, relevant for visibility and climate) globally. We find that domestic emissions contribute substantially to surface aerosol concentrations (57–95%) over all regions, but are responsible for a smaller fraction of AOD (26–76%). We define "background" aerosols as those aerosols over a region that result from inter-continental transport, DMS oxidation, and emissions from ships or volcanoes. Transport from other continental source regions accounts for a substantial portion of background aerosol concentrations: 36–97% for surface concentrations and 38–89% for AOD. We identify the Region of Primary Influence (RPI) as the source region with the largest contribution to the receptor's background aerosol concentrations (or AOD). We find that for dust Africa is the RPI for both aerosol concentrations and AOD over all other receptor regions. For non-dust aerosols (particularly for sulfate and BC), the RPIs for aerosol concentrations and AOD are identical for most receptor regions. These findings indicate that the reduction of the emission of non-dust aerosols and their precursors from an RPI will simultaneously improve both air quality and visibility over a receptor region.



## 1. Introduction

Human exposure to fine aerosols (particles with diameters less than 2.5 μm, $PM_{2.5}$), including sulfate ($SO_4^{2-}$), black carbon (BC), organic carbon (OC), and fine dust, and the associated adverse impacts on public health are of concern around the globe (Davidson et al., 2005; TF-HTAP, 2007). In addition, the release and transport of those aerosol species will change the optical properties of the atmosphere, resulting in the reduction of visibility and changes in regional and global climate (Park et al., 2004; Koch et al., 2007a,b; Levy et al., 2008).

Both observational and modeling studies show that aerosol concentrations are influenced by long-range transport as well as by domestic anthropogenic and natural emissions (Jacob et al., 2003; Jaffe et al., 2003; Park et al., 2003; Derwent et al., 2004; Heald et al., 2006; Chin et al., 2007; Liu and Mauzerall, 2007; TF-HTAP, 2007). Foreign anthropogenic emissions are considered to be part of background concentrations – the concentration in the absence of local emissions. Rising global emissions (particularly in developing countries), combined with meteorological conditions favorable for inter-continental transport, may make domestic efforts to control aerosol concentrations alone inadequate. For example, Park et al. (2004) found that trans-Pacific transport of Asian emissions accounted for nearly 30% of background concentrations of sulfate

* Correspondence to: Junfeng Liu, GFDL/NOAA, Princeton University Forrestal Campus, 201 Forrestal Road, Princeton, NJ 08540-5063, USA. Tel.:+1 609 452 5346; fax: +1 609 987 5063.
** Correspondence to: Denise L. Mauzerall, Department of Civil and Environmental Engineering and the Woodrow Wilson School of Public and International Affairs, Princeton University, 406 Robertson Hall, Princeton, NJ 08544, USA. Tel.: +1 609 258 2498.
*E-mail addresses:* Junfeng.Liu@noaa.gov (J. Liu), mauzeral@princeton.edu (D.L. Mauzerall).

1352-2310/$ – see front matter © 2009 Elsevier Ltd. All rights reserved.
doi:10.1016/j.atmosenv.2009.03.054

over the US and suggested that national visibility standards will be difficult to achieve without international controls. In addition, Liu et al. (2005) and Chin et al. (2007) described how air pollution emitted from Africa and Europe can travel eastward, merging with Asian pollution and crossing the North Pacific to influence air quality over western North America.

In order to understand the extent to which local air quality is compromised by foreign emissions, policymakers are increasingly interested in the source-receptor (S–R) relationships of inter-continental transport of air pollutants (Grennfelt and Hov, 2005), which are mostly quantified by atmospheric chemistry transport models (Park et al., 2004; Heald et al., 2006; Chin et al., 2007; Hadley et al., 2007; Koch et al., 2007b; Liu and Mauzerall, 2007; Liu et al., 2008; Saikawa et al., 2009). Recently, as coordinated by the United Nations' Task Force on Hemispheric Transport of Air Pollution (TF HTAP, http://www.htap.org), multi-model studies are being conducted to quantify and examine uncertainties in inter-continental S–R relationships for $O_3$, nitrogen deposition, aerosols, and other pollutants (TF-HTAP, 2007; Sanderson et al., 2008; Shindell et al., 2008; Fiore et al., 2009).

Our study uses a global 3D atmospheric chemistry transport model to simulate inter-continental transport of fine aerosols, including sulfate, black carbon, organic carbon and mineral dust aerosols (sea-salt and nitrate aerosols are neglected due to lack of a land source and negligible contribution to inter-continental transport, respectively (Malm et al., 1994; Park et al., 2004; Chin et al., 2007)). This paper is the first of two companion papers. Here, we first describe our model configuration (Section 2) and evaluate the simulations with global networks of aerosol observations (Section 3). We then present aerosol inter-continental source-receptor relationships for surface air quality and aerosol optical depth among ten continental regions (Section 4). Conclusions are in Section 5. In the companion paper (Liu et al., submitted for publication), we evaluate the impact of inter-continental transport of fine aerosols on global premature mortality.

## 2. Methods

### 2.1. Model description

We use the three-dimensional global chemical transport model MOZART-2 (Model of Ozone and Related Tracers, version 2) driven with NCEP/NCAR reanalysis meteorology from 1997 to 2003 (provided every 6 h) to simulate the global distribution of sulfate, BC, OC (with no secondary organic aerosols), and mineral dust aerosols. MOZART-2 includes a detailed photochemical mechanism for ozone, nitrogen oxides and hydrocarbons which is described and evaluated by Horowitz et al. (2003). In addition, several aerosol species have been added to MOZART-2 to represent the mass concentration of sulfate, BC, OC, ammonium nitrate and mineral dust (Tie et al., 2001; Tie et al., 2005). The model is configured with a T62 ($1.9^\circ \times 1.9^\circ$) horizontal resolution and 28 hybrid vertical levels from the surface to 2.7 mb (including 5 levels in the boundary layer and 7 levels above 100 hPa).

MOZART-2 includes sulfate production both by gas-phase oxidation of $SO_2$ by OH radicals and by aqueous phase oxidation of $SO_2$ by $H_2O_2$ (Martin and Damschen, 1981) and $O_3$ (Feichter et al., 1996). In addition, naturally produced dimethyl sulfide (DMS) can be oxidized to $SO_2$ by gas-phase reactions with OH and $NO_3$ radicals. Aqueous oxidation of $SO_2$ to sulfate depends on cloud water content, acidity of cloud water, temperature, and abundance of oxidizing agents (namely $H_2O_2$ and $O_3$). When clouds are present, MOZART-2 first predicts the pH values based on the mixing ratios of $SO_2$, $CO_2$, $HNO_3$, sulfate, and $NH_3$. It then uses the predicted pH and temperature to calculate the temperature dependent effective Henry's Law constants and aqueous reaction rate coefficients (Tie et al., 2005). When the cloud pH is below 5, the reaction rate between $SO_2$ and $H_2O_2$ is much faster than that between $SO_2$ and $O_3$ (Seinfeld and Pandis, 1998; Brasseur et al., 1999).

Black carbon (BC) and organic carbon (OC) are each represented by two model species, namely hydrophobic (BC1/OC1) and hydrophilic carbon (BC2/OC2) (Cooke et al., 2002). Emissions from combustion and biomass burning are initially a mixture of hydrophobic and hydrophilic carbon; hydrophobic carbon is gradually coated by sulfate and other components to form hydrophilic carbon (Tie et al., 2005). We convert hydrophobic to hydrophilic carbon with a 1.6-day timescale as an approximation for the above processes which are not explicitly represented in the model (Tie et al., 2005). The simulation of dust from natural sources generally follows (Ginoux et al., 2001; Zender et al., 2003; Ginoux et al., 2006). Five bins are used to resolve the size distribution of dust (diameter ranges of 0.2–2 μm, 2–3.6 μm, 3.6–6 μm, 6–12 μm, and 12–20 μm, see Table 1). The simulation of dust entrainment depending on wind speed follows the microphysical approach developed by Marticorena and Bergametti (1995).

Removal processes for aerosols include both dry deposition and wet scavenging. The dry deposition velocities for $SO_2$ are from Feichter et al. (1996) and are much faster over ocean (0.8 cm $s^{-1}$) and land (0.6 cm $s^{-1}$) than over snow (0.2 cm $s^{-1}$). The dry deposition velocities for sulfate and carbonaceous aerosols are 0.2 cm $s^{-1}$ (Feichter et al., 1996) and 0.1 cm $s^{-1}$ (Cooke and Wilson, 1996) over all surfaces, respectively. Dry deposition for dust aerosols includes both vertical gravitational settling (Seinfeld and Pandis, 1998) and dry turbulent mixing out at the surface (Giorgi, 1986). Wet deposition includes both in-cloud rainout and below cloud washout (Horowitz et al., 2003). In MOZART-2, the wet deposition rate for $SO_2$ is set equal to that of $H_2O_2$ (Tie et al., 2005; Liu et al., 2008). For sulfate and hydrophilic carbon (BC2/OC2), the wet deposition rates are set to 20% of that for the highly soluble gas $HNO_3$ (Horowitz, 2006). Wet deposition for dust is based on scavenging efficiencies from Zender et al. (2003).

In MOZART-2, sulfate and carbonaceous aerosols are simulated as $SO_4^{2-}$ and carbon mass. In order to calculate the total mass of these aerosols, we assume that sulfate aerosols are composed of ammonium sulfate and that the ratio of organic mass (OM) to organic carbon is 1.3 for hydrophobic and 1.7 for hydrophilic OC (Ming et al., 2005). We compare simulated and observed OC concentrations in the model evaluation section but report OM ($OM = 1.3 \cdot OC1 + 1.7 \cdot OC2$) in the results section of the paper. The mass fraction of PM2.5 is calculated online, assuming lognormal size distributions with dry mode mean diameters and geometric standard deviations for sulfate, BC and OC from Chin et al. (2002). In addition, hygroscopic growth (i.e., aerosol growth by absorbing ambient moisture) for hydrophilic aerosols (i.e., sulfate, BC2, and OC2) is calculated online using growth factors (as a function of relative humidity) from Chin et al. (2002) and influences the amount of aerosol particles below 2.5 μm diameter. Hygroscopic growth of dust particles is ignored. PM2.5 mass concentrations for

**Table 1**
Global budget of mineral dust.

| | Size (diameter), μm | Annual emissions, Tg $year^{-1}$ | Avg. load, Tg | Avg. lifetime, days |
|---|---|---|---|---|
| Dust1 | 0.2–2.0 | 111 | 5.1 | 17 |
| Dust2 | 2.0–3.6 | 210 | 6.0 | 11 |
| Dust3 | 3.6–6.0 | 322 | 4.2 | 4.8 |
| Dust4 | 6.0–12 | 581 | 2.0 | 1.3 |
| Dust5 | 12–20 | 437 | 0.46 | 0.4 |
| Dust1–5 | 0.2–20 | 1661 | 17.8 | 3.9 |

dust are obtained by summing the first (0.2–2 μm) and 29% of the second (2–3.6 μm) dust size bins.

### 2.2. Emissions

Anthropogenic emissions (including $SO_2$, $NO_x$, CO, $NH_3$, and NMVOCs) are based on the RAINS (Regional Air Pollution Information and Simulation) model CLE (i.e., Current Legislation) emission inventory for the year 2000, which was developed at the International Institute for Applied Systems Analysis (IIASA) using the global version of the RAINS model. These emissions include industrial, residential, and road emissions. The CLE inventory was used by Dentener et al. (2005) to evaluate the response of tropospheric ozone and radiative forcing to the change of emissions from 1990 to 2030. In addition, Dentener et al. (2006) and Stevenson et al. (2006) used the CLE inventory in 26 global atmospheric chemistry models to assess the change of the global atmospheric environment between 2000 and 2030. Biomass burning emissions are from van der Werf et al. (2003, 2004), based on an average of their 1997–2002 emissions. DMS emissions are from the Global Emissions Inventory Activity (GEIA) (Benkovitz et al., 1994; Benkovitz et al., 1996). Black and organic carbon emissions are from Bond et al. (2004) and include 1996 emissions from fossil fuel combustion and biofuels and open field biomass burning (representative of the mid-1990s). However, BC and OC emissions in the Bond et al. (2004) inventory only account for aerosols with diameter less than 1μm. We scaled BC emissions by 1.15 and OC emissions by 1.4 to account for total BC and OC emissions (Cooke et al., 1999; Bond et al., 2004). We assume 80% of BC and 50% of OC are emitted as hydrophobic carbon with the rest emitted as hydrophilic carbon, similar to Cooke et al. (1999). We neglect the production of secondary organic aerosols (SOA), which are estimated to contribute an additional 20–30 Tg $year^{-1}$ (Heald et al., 2008; Henze et al., 2008).

Dust entrainment is calculated online, depending on land type and surface wind stress (Ginoux et al., 2001; Zender et al., 2003). The dust source function which estimates the fraction of alluvium available for wind erosion is from Ginoux et al. (2001). The clay fraction is set to 0.2 (suggested by Zender et al. (2003)) for dust sources which are characterized by deposits of alluvium. A trimodal lognormal size distribution for wind-carried dust is configured as recommended by d'Almeida et al. (1991).

In order to compare the relative importance of regional aerosol emissions, we define ten continental regions as shown in Fig. 1: North America (NA), South America (SA), Europe (EU), the Former Soviet Union (FSU, excluding part of Russia in the European domain), Africa (AF), Indian Subcontinent (IN), East Asia (EA), Southeast Asia (SE), Australia (AU), and the Middle East (ME). Fig. 2a compares the magnitudes of total sulfur (excluding DMS), BC, OC and fine dust emissions from these ten continental regions. Globally, the dominant source of aerosols is fine dust which comes primarily from Africa. In addition, OC emissions from biomass burning in AF and SA, as well as anthropogenic $SO_2$ emissions from EA, NA and EU are much higher than from other regions.

In this study, biomass burning and industrial emissions are distributed vertically above the surface, with other emissions released at the surface. Specifically, we distribute biomass burning emissions up to 5000 m (>99% below 2000 m) from the surface using the vertical profile from van der Werf et al. (2003). For industrial emissions, according to United States Good Engineering Practices (GEP), stack heights should not be lower than 65 m. Other countries may have different standards for the height of industry stacks. In order to represent an average situation for the stack height as well as account for plume buoyancy, we assume that all industrial emissions are evenly distributed between the surface and 500 m (the heights for the tops of the eight lowest levels in MOZART-2 are approximately 80 m, 210 m, 380 m, 580 m, 840 m and 1160 m, 1550 m, and 2020 m).

The anthropogenic emissions as well as BC and OC emissions described above lack seasonality. In this study, we seasonalize anthropogenic $SO_2$ and $NO_x$ emissions according to Global Emissions Inventory Activity (GEIA). The seasonality of BC and OC emissions are treated separately by source. For emissions from fossil fuel combustion, we use the seasonality of anthropogenic CO emissions. For open burning, the seasonality of BC and OC emissions is based on $CO_2$ emissions from biomass burning from the IMAGES model (Muller, 1992; Muller and Brasseur, 1995). For biofuel emissions, seasonality is based on Heating Degree Days (HDD) (Cabada et al., 2002). In addition, no diurnal or week day/weekend variations are included. The resulting seasonal variation of anthropogenic BC emissions (including fossil fuel and biofuel sources) from the ten continental regions is shown in Fig. 2b, and is comparable to the seasonality used by Park et al. (2003).

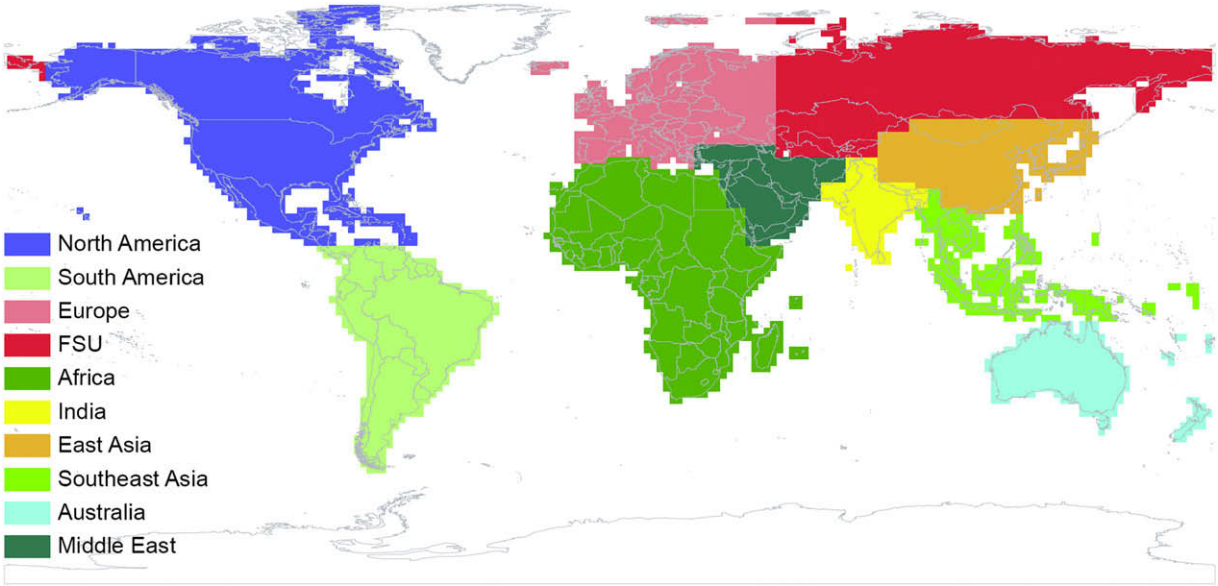


**Fig. 1.** The ten continental regions tagged in our MOZART-2 simulations.

### 2.3. Tagged regional tracers

We tag aerosols and their precursors (i.e., $SO_2$, sulfate, mineral dust, BC1, BC2, OC1 and OC2) by region and source type when they are emitted. The ten continental regions are shown in Fig. 1. In addition, we use the ROW (rest of the world) tracer to represent the emissions from ships and untagged regions in Fig. 1. For $SO_2$ and sulfate, only anthropogenic emissions are tagged because $SO_2$ is dominated by anthropogenic sources. To characterize the contribution of DMS to sulfate concentrations, we use two additional tracers to account for $SO_2$ and sulfate formation from oxidation of DMS. For carbonaceous aerosols (i.e., BC1, BC2, OC1 and OC2), we tag both anthropogenic and biomass burning emissions because substantial quantities of BC and OC emissions originate from biomass burning (much of which is of anthropogenic origin). For mineral dust, we tag dust particles in each of five size bins. Tagged tracers do not perturb the chemistry of the system, but follow the physical and chemical evolution of each process. We evaluate our tagging procedure by comparing the sum of the tagged tracers of a specific species with the concentration of the same untagged species. In general, the difference in most locations is less than 1%, with up to 3% discrepancies in a few locations likely due to numerical errors and nonlinear calculations in model parameterizations (e.g. advection, convection, diffusion, and heterogeneous reactions).

### 2.4. Aerosol optical depth

In this study, we calculate the aerosol optical depth (AOD) at 550 nm, using the methodology of (Ginoux et al., 2006). For each aerosol species, the aerosol optical depth is the product of aerosol dry mass concentrations and the specific extinction coefficients (which depend on the relative humidity (RH)). Specific extinction coefficients at any RH are precalculated from Mie theory on the basis of aerosol size distributions, refractive indices, particle density, and hygroscopic properties (these properties for sulfate and black carbon are described in detail by (Haywood and Ramaswamy, 1998)), and are provided as a "look-up" table. The total AOD is calculated by summing the AOD in each model layer for each aerosol species using the assumption that they are externally mixed. A more detailed description of the AOD calculation is given by Ginoux et al. (2006).

## 3. Model evaluation

Aerosol distributions simulated by MOZART-2 driven with the Middle Atmosphere Community Climate Model (MACCM-3) winds and EDGAR-2 emission inventories are described by Horowitz et al. (2003) and Tie et al. (2005) and are evaluated with observations by Ginoux et al. (2006). Simulated aerosol concentrations are generally within a factor of 2 of the observations (Ginoux et al., 2006). This study uses meteorological fields from the NCEP reanalysis (rather than MACCM-3) and the RAINS-CLE-2000 emission inventory (rather than EDGAR-2). We evaluate our simulated aerosol concentrations by comparing a 7-year average of model results with various observational data for sulfate, BC, OC, and dust, and then place our results in the context of previous modeling studies. The annual total emissions, average atmospheric mass loading, and average lifetimes of dust, sulfate, BC, OC aerosols are listed in Tables 1 and 2. Due to paper length limits, detailed model evaluation (including both annual mean and seasonal variability) is given in the auxiliary material (see Part-II

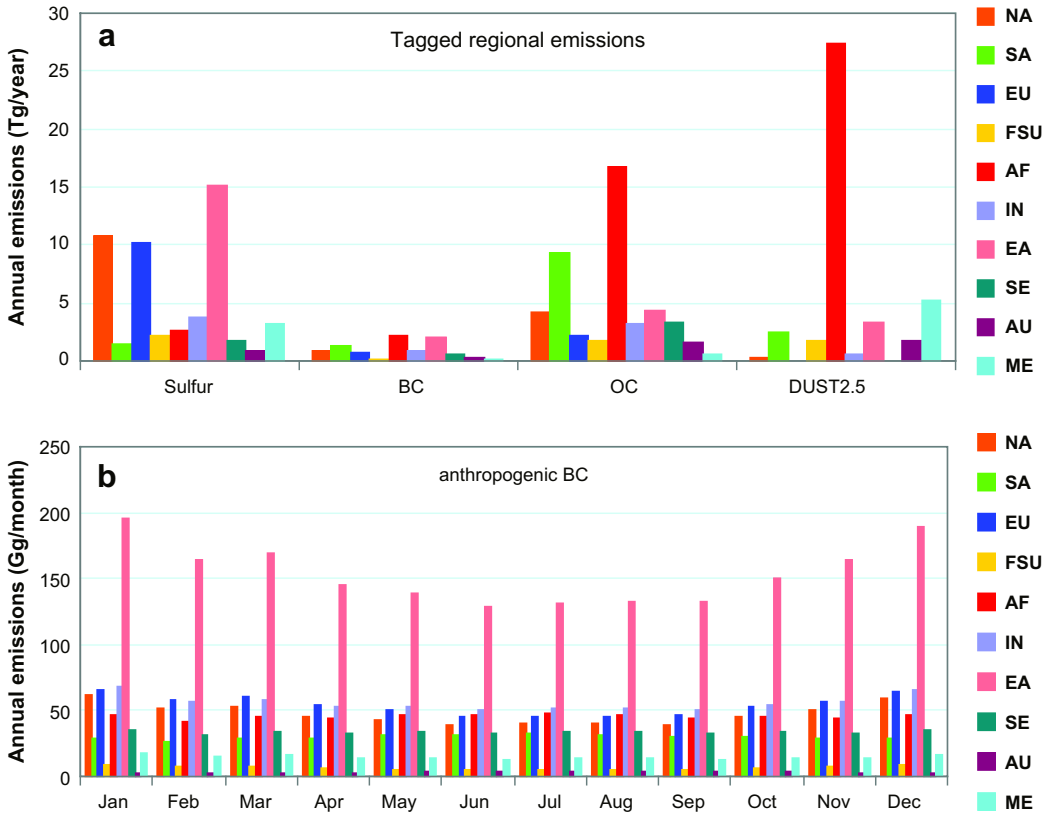


**Fig. 2.** Regional emissions. (a) Annual total emissions from ten continental regions of sulfur (TgS year$^{-1}$), black carbon (TgC year$^{-1}$), organic carbon (TgC year$^{-1}$) and fine dust (PM2.5, $10^{13}$ g year$^{-1}$). (b) Monthly emissions of anthropogenic black carbon (including fossil fuel and biofuel sources) from ten continental regions (Gg month$^{-1}$).

**Table 2**
Global budget of sulfate, BC and OC aerosols.

| | Annual Emissions,[a] Tg year$^{-1}$ | Avg. load, Tg | Avg. lifetime, days |
|---|---|---|---|
| Sulfate | 40.2[b] | 0.61 | 5.4 |
| BC | 9.2 | 0.17 | 5.8 |
| OC | 48[c] | 0.83 | 5.3 |

[a] Unit Tg means Tg S for sulfate, and Tg C for BC and OC.
[b] Total sulfate sources ($SO_4^{2-}$), including 1.1 TgS year$^{-1}$ from direct emissions, 9.6 TgS year$^{-1}$ from gas-phase $SO_2$ oxidation, and 29.5 TgS year$^{-1}$ from heterogeneous oxidation of $SO_2$.
[c] Secondary organic aerosols are not simulated in this study.

Detailed Model Evaluation). Here we briefly summarize the model evaluation.

The total sulfur emissions in this work are comparable to Chin et al. (2002). In addition, the average atmospheric mass loading and average lifetime for sulfate is 0.61 TgS and 5.4 days, close to Chin et al. (2002) (0.65 TgS and 6.1 days).

Fig. 3 compares simulated and observed annual mean sulfate concentrations. Observations were collected by the Rosenstiel School of Marine and Atmospheric Science (RSMAS) at the University of Miami (Prospero, 1996) and by three regional observation networks, namely the Interagency Monitoring of Protected Visual Environments (IMPROVE) in the United States (http://vista.cira.colostate.edu/IMPROVE/), the Cooperative Program for Monitoring and Evaluation of the Long-range Transmission of Air Pollutants in Europe (EMEP: http://www.emep.int), and the East Asian Monitoring Network (EANET: http://www.eanet.cc). We average observations over the 1980s–1990s for RSMAS data, over 1997–2003 for IMPROVE and EMEP data, and over 2000–2004 for EANET (since many EANET observation stations did not begin to report data until 2003). The simulated sulfate concentrations are in general within a factor of 2 of the observations, but tend to underestimate the observations at stations in California, along the US-Mexico border, eastern Russia and some tropical areas, and to overestimate summer sulfate concentrations in some European countries (e.g. Ireland, Iceland, Norway, Sweden) and Southeast Asian countries as well as most sites in the southern hemisphere (Fig. 3). Possible explanations include the biases from wet deposition (Horowitz, 2006) as well as that some of the RSMAS observations include data from the early 1980s, when global emissions were quite different than those in 2000. Between the 1980s and 2000s substantial decreases of $SO_2$ emissions occurred in Europe and the United States while $SO_2$ emissions increased rapidly in South and East Asia as well as the developing countries in the Southern Hemisphere. For example, observations from Hedo, Japan (based on both RSMAS and EANET data) indicate that the change in sulfate concentrations over Japan likely reflects both increases in $SO_2$ emissions from mainland EA and decreases in local Japanese $SO_2$ emissions from the early 1990s to the early 2000s (see detailed discussion in the supplementary material). Furthermore, high sulfur concentrations over Southeast Asia are partly due to frequent volcanic emissions which are treated as surface emissions in MOZART-2.

The BC and OC emissions used in this study (from Bond et al. (2004)) are approximately half those of Chin et al. (2002) and Park et al. (2003). As a result, the mass loading of BC and OC is in general lower than other studies by 40–50%. The average lifetimes of BC and OC are 5.8 and 5.3 days in this work, comparable to Chin et al. (2002) (6.2 days for BC, and 5.1 days for OC).

Simulated BC and OC concentrations are compared with both IMPROVE (Fig. 4a and c) and EMEP observations (Fig. 4b and d). Simulated BC and OC concentrations in general agree within a factor of 2 with the IMPROVE observations (including fine elementary carbon and fine organic carbon) but tend to be systematically underestimated in many places, particular over California and in the southeastern U.S. This is probably due to errors in the BC and OC emissions (particularly in biomass burning emissions). In addition, the underestimate of OC concentrations may also be caused by the lack of secondary organic aerosols in our simulation (Cooke et al., 1999; Heald et al., 2005). BC and OC data from EMEP are from July 2002 to June 2003. As shown in Fig. 4b, our simulated BC concentrations generally agree within a factor of 2 with the EMEP observations. However, our model systematically underestimates OC concentrations over the EU by a factor of 2 (Fig. 4d), probably due to the lack of secondary organic aerosols (Cooke et al., 1999).

The annual total dust emissions in this study are 1661 Tg year$^{-1}$, comparable to those of other studies (Ginoux et al., 2001; Chin et al., 2002; Zender et al., 2003). However, the average dust loading

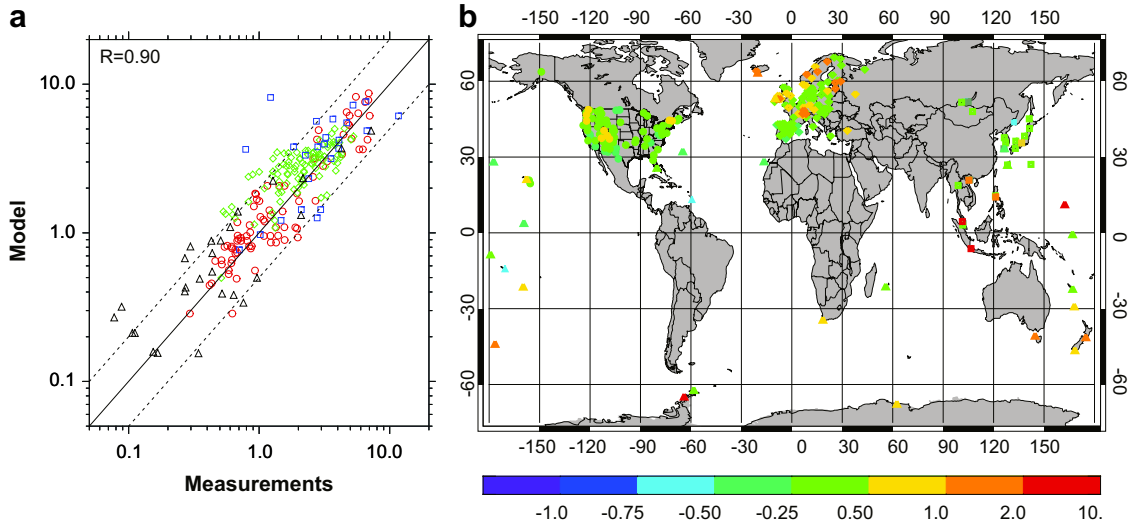


**Fig. 3.** (a) Scatter plot and (b) the relative difference (i.e., (model-measurement)/measurement, right panel) between the simulated (MOZART-2, 1997–2003 average) and observed annual mean sulfate concentrations ($SO_4^{2-}$; μg m$^{-3}$). Measurements are from RSMAS (1980s–1990s average, University of Miami, black triangles), IMPROVE (1997–2003 average, the United States, red circles), EMEP (1997–2003 average, Europe, green diamonds), and EANET (2000–2004 average, East and Southeast Asia, blue squares). Shapes in the right panel, as described above, indicate the network from which the measurements originate.

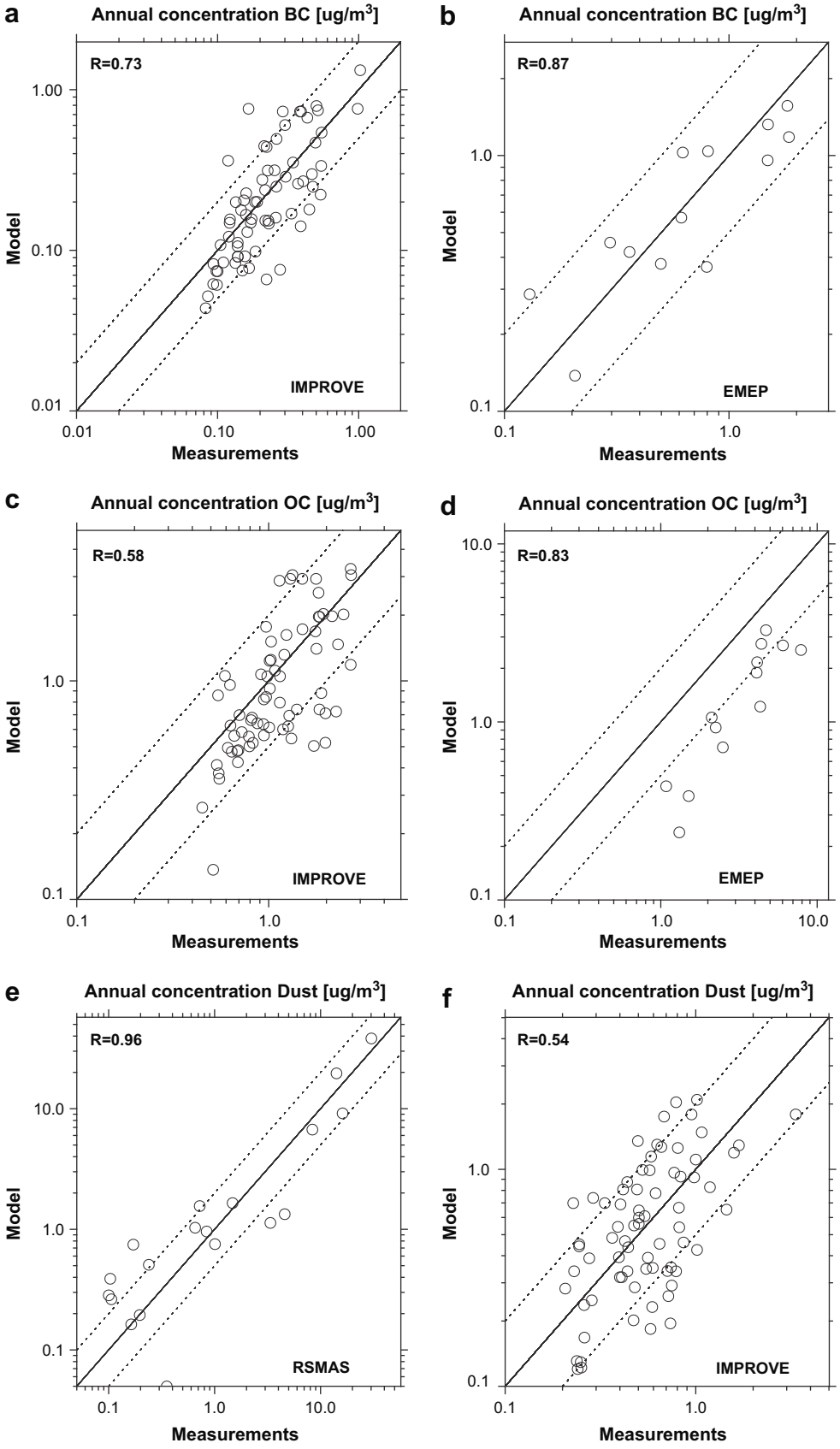


**Fig. 4.** Same as Fig. 3a, but for BC (a,b), OC (c,d), and dust (e,f) concentrations. Measurements are from IMPROVE (a,c,f, 1997–2003 average), EMEP (b,d, 2002–2003 average), and University of Miami, RSMAS (e, 1980s–1990s average). The solid line represents 1:1 line, indicating modeling results are equal to measurements. The two dashed lines are (2:1) and (1:2) lines, indicating the modeling results are twice (2:1) or half (1:2) of the measurements.

is 17.8 Tg, which is lower than Chin et al. (2002) (21 Tg) and Ginoux et al. (2001) (35.9 Tg). The lower dust loading is because we include larger dust size bins which lead to a shorter dust lifetime than the earlier work. Our average lifetime for dust particles is 3.9 days, close to Zender et al. (2003) (4.3 days), but lower than Chin et al. (2002) (5.1 days) and Ginoux et al. (2001) (7.1 days), mainly because they are using smaller dust sizes (i.e., 0.2–12 μm in diameter).

Fig. 4e compares simulated dust concentrations with observed dust concentrations collected by the University of Miami (compiled by Mahowald et al. (2006)). The simulated dust concentrations in general agree within a factor of 2 of the observations, except that they underestimate dust concentrations in Florida and Bermuda in summer by a factor of 2–3. We also compare simulated submicron dust concentrations with the IMPROVE observations (Fig. 4f). Model simulations in general agree within a factor of 2 of the observations and capture the seasonal cycle of submicron dust concentrations. More detailed model evaluation is in the auxiliary material.

## 4. Source-receptor relationships

We quantify and compare the source-receptor relationships for fine surface aerosol concentration (SAC) and aerosol optical depth (AOD, based on total aerosol concentrations) due to the inter-continental transport of aerosols among ten continental regions. Surface concentrations indicate the relative importance of the inter-continental transport of aerosols on a region's surface air quality. Aerosol optical depth is an indicator of the reduction in incoming solar radiation (at a particular wavelength) due to the scattering and absorption of sunlight by aerosols. It is the basis from which changes in visibility and radiative forcing can be calculated. We average the simulated aerosol concentration distributions between 1997 and 2003 to represent an average distribution around 2000. Global distributions of SAC and AOD of sulfate, BC, Organic Mass (OM) and dust aerosols from each continental region are shown in the auxiliary materials (see Figs. A1–A4 for SAC and Figs. A5–A8 for AOD).

### 4.1. Surface aerosol concentrations (SAC)

In this study, we define the background concentration to be the total concentration over a receptor region resulting from all sources except emissions from the receptor region. Domestic emissions are defined here to be those from a particular source region and include only anthropogenic sulfur emissions, natural dust emissions, and both anthropogenic and biomass burning emissions for carbonaceous aerosols. Therefore, for a receptor region background sources include contributions from inter-continental sources (i.e., the nine foreign regions), as well as emissions from ships, volcanoes, biomass burning (sulfate only), and DMS (sulfate only) which are denoted as ROW (rest of world). (Note: the definition of background concentration in this study is different from that of Park et al. (2004) and Chin et al. (2007).)

#### 4.1.1. Relative importance of source regions and aerosol types

Table 3 summarizes the area-weighted (A-W, see definition in Equation (1)) simulated fine aerosol (PM2.5: including fine sulfate, BC, OM and dust) surface concentrations for each receptor region, including contributions from domestic and background sources. In addition, for each receptor region, the percent contribution of each aerosol type to the total is also provided.

$$C_{AW} = \frac{\sum_{i=1}^{K} C_i \cdot S_i}{\sum_{i=1}^{K} S_i} \quad (1)$$

where $C_{AW}$ is the area-weighted aerosol concentration over a receptor region R; $C_i$ is the aerosol concentration in grid box $i$ in R; $S_i$ is the area of grid box $i$ in R. $K$ is the total grid boxes covered by R.

Among the ten receptor regions, the A-W annual average SAC of PM2.5 ranges from more than 4 $\mu g\,m^{-3}$ (over NA) to around 26 $\mu g\,m^{-3}$ (over AF). NA, FSU, SE, AU, SA and EU are among the receptors with low PM2.5 levels ($<8\ \mu g\,m^{-3}$); while PM2.5 is much higher in the AF, ME, EA and IN regions ($>16\ \mu g\,m^{-3}$), mostly due to fine dust aerosols.

Over NA and EU, nearly 80% of the total PM2.5 is attributed to anthropogenic sulfate and OM aerosols. In contrast, for AF and the ME, more than 80% of surface PM2.5 is fine dust. Emissions from within the region account for more than 90% of total PM2.5 in AF and AU, around 80–85% in NA, SA and EA, and less than 70% in the EU, FSU, ME, IN, and SE regions. For background PM2.5, fine dust is usually a dominant component (~40–80%) and sulfate aerosol ranks second (~30–50%). Contributions from carbonaceous aerosols (5–15%) and sulfate from DMS oxidation (~2–15%) are small in most receptor regions. For all receptors except SA and AU, inter-

**Table 3**
Contributions to annual average area-weighted fine aerosol (PM2.5) surface aerosol concentrations (SAC) (units: $\mu g\,m^{-3}$) over each receptor region. 'Total' indicates total fine aerosol (PM2.5) concentrations including ammonium sulfate, black carbon (BC), organic mass (OM), and fine dust; 'Domestic' indicates aerosol concentrations resulting from local emissions (a list of domestic sources is in Section 4); Background is the difference between 'Total' and 'Domestic' concentrations. The percent contribution from each aerosol species to each category (i.e., 'Total', 'Domestic', 'Background') is also quantified. Note: "DMS" represents sulfate aerosols derived from DMS, while "Sulfate" in the 'Background' category represents sulfate contributed from ROW (ROW = ships, airplanes, volcanoes, etc.).

| | Sources | Unit | Receptors | | | | | | | | | |
|---|---|---|---|---|---|---|---|---|---|---|---|---|
| | | | NA | SA | EU | FSU | AF | IN | EA | SE | AU | ME |
| **Total** | | **$\mu g\,m^{-3}$** | **4.4** | **6.1** | **7.6** | **4.6** | **25.9** | **16.4** | **17.7** | **5.0** | **5.8** | **25.2** |
| | Sulfate | % | 49 | 18 | 48 | 25 | 5 | 20 | 29 | 40 | 13 | 12 |
| | BC | % | 5 | 5 | 7 | 2 | 1 | 5 | 6 | 6 | 2 | 1 |
| | OM | % | 33 | 49 | 27 | 22 | 12 | 30 | 22 | 41 | 21 | 4 |
| | Dust | % | 14 | 28 | 18 | 50 | 82 | 45 | 43 | 13 | 64 | 83 |
| **Domestic** | | **$\mu g\,m^{-3}$** | **3.6** | **5.0** | **5.2** | **3.2** | **24.3** | **9.7** | **15.1** | **2.8** | **5.2** | **15.2** |
| | Sulfate | % | 50 | 10 | 53 | 18 | 1 | 28 | 29 | 31 | 7 | 12 |
| | BC | % | 5 | 6 | 9 | 2 | 1 | 8 | 7 | 8 | 2 | 1 |
| | OM | % | 39 | 59 | 38 | 28 | 12 | 48 | 23 | 61 | 23 | 4 |
| | Dust | % | 5 | 25 | 0 | 51 | 85 | 16 | 41 | 0 | 68 | 83 |
| **Background** | | **$\mu g\,m^{-3}$** | **0.8** | **1.1** | **2.4** | **1.5** | **1.7** | **6.7** | **2.6** | **2.2** | **0.6** | **10.0** |
| | Sulfate | % | 28 | 37 | 28 | 36 | 42 | 8 | 30 | 48 | 17 | 11 |
| | BC | % | 1 | 0 | 1 | 2 | 1 | 0 | 2 | 3 | 1 | 1 |
| | OM | % | 4 | 5 | 5 | 10 | 9 | 4 | 15 | 15 | 9 | 3 |
| | Dust | % | 52 | 42 | 58 | 46 | 41 | 87 | 51 | 30 | 27 | 84 |
| | DMS | % | 15 | 16 | 8 | 5 | 7 | 2 | 2 | 3 | 46 | 1 |

continental sources account for more than 60% of background PM2.5 with the remainder coming from ships, airplanes, volcanoes and DMS oxidation. Background PM2.5 concentrations are 0.8, 2.4, 2.6, and 6.7 $\mu g\,m^{-3}$ over NA, EU, EA and IN regions, respectively, with 63% (NA), 76% (EU), 85% (EA) and 97% (IN) of background PM2.5 attributed to "inter-continental" sources. Fine dust dominates (>75%) the inter-continental sources, particularly in NA, SA, EU, IN and the ME (see Table 3 as well as Table A1 in the supplementary material).

#### 4.1.2. Region of primary influence (RPI)

For environmental policy it is useful to understand which foreign region's emissions have the largest effect on a receptor region's air quality. Here we define this source region as the Region of Primary Influence (RPI) on that receptor region. The inter-continental influence patterns depicted by the RPIs are intended to illustrate key trans-boundary air pollution transport patterns and thus inform discussion on the design of possible future regional, hemispheric or global environmental agreements to address them.

Fig. 5 illustrates the inter-continental influence pattern based on the RPI for SAC. AF is the dust RPI for all other regions and particularly for the ME (more than 70% of dust in the ME of inter-continental origin is from AF), IN, EU (most of the influence occurs over the southern EU), SA (mostly over northern SA) and NA (with largest influence on southern NA, particularly on the Southeastern U.S. Using A-W concentrations over a continental region to determine RPI will mask sub-regional variability in the foreign contributions; see Fig. A4 in the supplementary material for sub-regional dust distributions). EA is NA SAC RPI for sulfate, BC and OM aerosols (with the largest influence on the western U.S.) indicating that the trans-pacific transport of EA aerosols (excluding dust) is the major foreign source of non-dust PM2.5 to NA. This is consistent with findings from (Park et al., 2004; Liu and Mauzerall, 2005; Chin et al., 2007; Liu and Mauzerall, 2007; Liu et al., 2008). The RPI is the same for sulfate, BC and OM aerosols for EU → FSU (i.e., EU is the FSU's RPI), EU → AF, ME → IN, EA → SE, and AF → AU (Fig. 5, sub-regional distribution is illustrated in Fig. A1–A4 in the supplementary material). However, for the SA, EU, EA and ME receptors, each aerosol species (i.e., sulfate, BC or OM) can have a different RPI. For example, the RPI for EA SAC is the FSU (for sulfate and OM) and IN (for BC). More detailed inter-continental source-receptor relationships for aerosols are in Table A1 of the supplementary material.

### 4.2. Aerosol optical depth (AOD)

To establish the source-receptor relationships for AOD, we calculate the AOD resulting from the inter-continental transport of aerosols (as described in Section 2.4). Table 4 summarizes the composition of AOD averaged over each receptor region. The horizontal distribution of AOD for each aerosol species from each source region are shown in Figs. A5–A8. The total AOD due to all-size sulfate, carbonaceous and fine dust aerosols is in the range 0.04 (over AU) to 0.16 (over EA). Background aerosols are a larger fraction of AOD than of SAC over most receptor regions. For example, over NA and EA, about 42% and 32%, respectively, of the total AOD originates from background aerosols. This is more than twice that of SAC for the same regions because after long-range transport the aerosol maximum occurs in the free troposphere above a receptor, while aerosols emitted domestically dominate SAC. For the FSU, ME and SE receptors, background AOD is larger than domestic AOD (i.e., approximately 60% of total AOD), mainly because those regions are

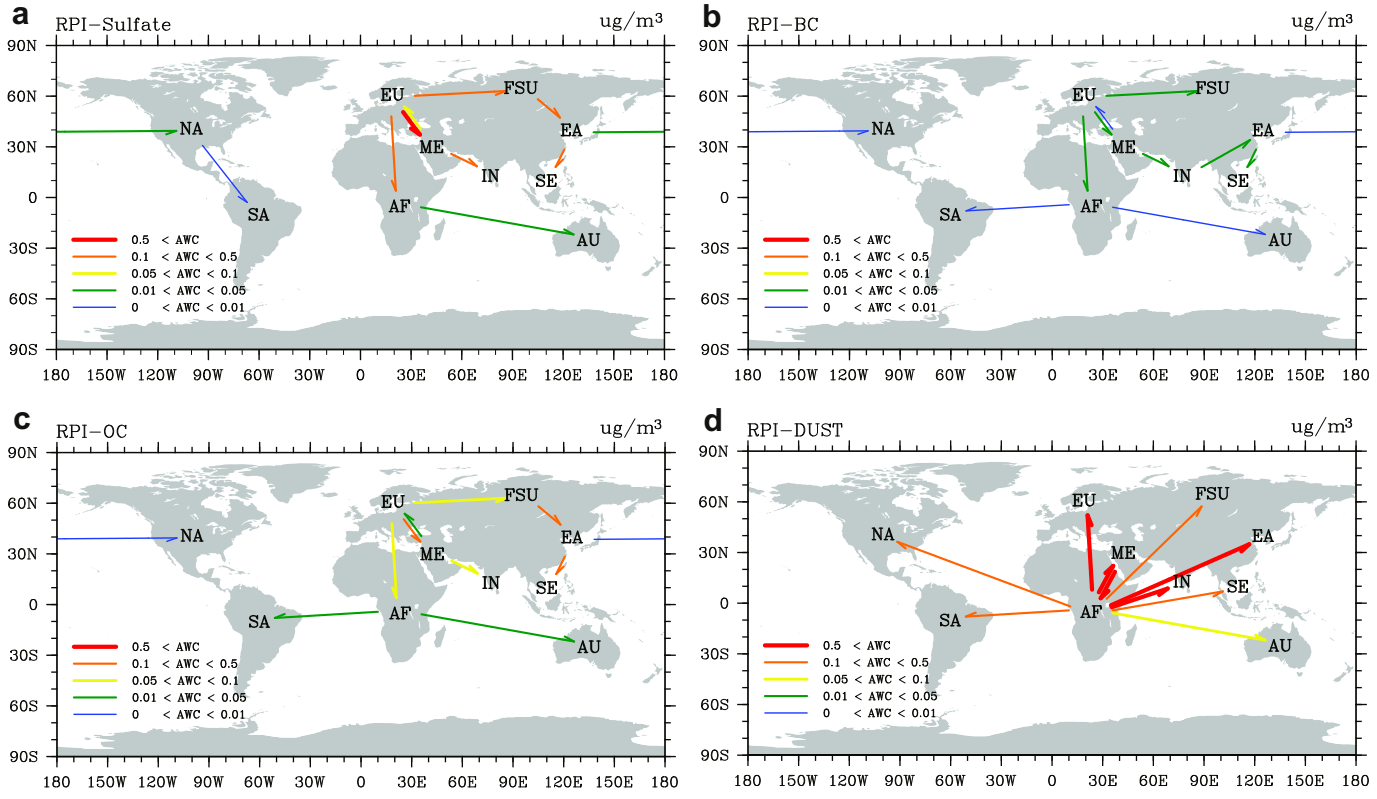


**Fig. 5.** Inter-continental influence patterns based on RPI, Region of Primary Influence (the largest foreign source region to influence a receptor) for SAC (surface aerosol concentrations) of (a) sulfate (b) black carbon (c) organic carbon and (d) fine mineral dust. Arrows point in the direction of influence from RPI to a receptor region. Colors indicate the magnitude of area-weighted surface concentrations (contributed from RPI) in the receptor region (unit: $\mu g\,m^{-3}$).

**Table 4**
Same as Table 3, but for area-weighted aerosol optical depth (AOD).

| | Sources | Unit | Receptors | | | | | | | | | |
|---|---|---|---|---|---|---|---|---|---|---|---|---|
| | | | NA | SA | EU | FSU | AF | IN | EA | SE | AU | ME |
| **Total** | | | **0.069** | **0.070** | **0.113** | **0.077** | **0.119** | **0.136** | **0.161** | **0.064** | **0.042** | **0.121** |
| | Sulfate | % | 64 | 36 | 68 | 64 | 19 | 41 | 57 | 56 | 36 | 41 |
| | BC | % | 6 | 8 | 7 | 5 | 6 | 9 | 10 | 8 | 7 | 5 |
| | OM | % | 23 | 47 | 17 | 19 | 36 | 31 | 23 | 30 | 40 | 15 |
| | Dust | % | 7 | 9 | 9 | 11 | 39 | 19 | 10 | 6 | 17 | 39 |
| **Domestic** | | | **0.040** | **0.044** | **0.061** | **0.020** | **0.091** | **0.080** | **0.110** | **0.027** | **0.022** | **0.049** |
| | Sulfate | % | 67 | 16 | 72 | 53 | 5 | 44 | 61 | 41 | 19 | 44 |
| | BC | % | 6 | 12 | 9 | 5 | 6 | 12 | 11 | 11 | 7 | 4 |
| | OM | % | 26 | 69 | 19 | 32 | 40 | 39 | 21 | 48 | 48 | 8 |
| | Dust | % | 1 | 3 | 0 | 10 | 48 | 5 | 7 | 0 | 26 | 44 |
| **Background** | | | **0.029** | **0.026** | **0.052** | **0.057** | **0.028** | **0.056** | **0.051** | **0.037** | **0.021** | **0.072** |
| | Sulfate | % | 45 | 47 | 51 | 61 | 50 | 30 | 45 | 59 | 26 | 36 |
| | BC | % | 5 | 2 | 4 | 6 | 5 | 5 | 6 | 6 | 6 | 5 |
| | OM | % | 18 | 11 | 14 | 15 | 20 | 19 | 27 | 17 | 31 | 20 |
| | Dust | % | 15 | 19 | 19 | 11 | 11 | 40 | 17 | 11 | 8 | 36 |
| | DMS | % | 16 | 20 | 12 | 7 | 13 | 7 | 5 | 7 | 28 | 4 |

located directly downwind of major aerosol source regions (i.e., EU, AF, and EA, respectively).

Sulfate aerosols dominate (~60%) total AOD over NA, EU, FSU, EA and SE (Table 4). OM accounts for nearly 40% of total AOD in SA, AF and AU, but is relatively small in other regions (≤31%; Table 4). Compared to SAC, the contribution of dust aerosols to the total AOD is relatively small (≤19%) in most regions except AF and the ME (where they account for nearly 40% of AOD). For all regions, less than 10% of total AOD is contributed from BC.

Inter-continental transport of aerosols contributes substantially to each receptor's background AOD (>60% except SA and AU, see Table 4 and Table A2 in the supplementary material). Unlike SAC (where dust dominates most regions' background SAC), sulfate accounts for nearly half of background AOD over NA, SA, EU, FSU, AF, EA and SE. To describe the key influence patterns, Fig. 6 illustrates each receptor region's RPI (i.e., the largest foreign source region to influence a receptor's AOD) based on inter-continental AOD for each aerosol species. Comparing Figs. 6–5, for each receptor region, the RPI is usually identical for AOD and SAC for dust or sulfate aerosols (except for the EA receptor, whose sulfate RPI is FSU for SAC, but is IN for AOD). However, for carbonaceous aerosols, the RPI differs for SAC versus AOD in the EU, AF, IN, EA, and SE receptors. For example, over the EU receptor, the RPI for SAC is ME for both BC and OM, but for AOD it is NA for these species. Similarly,

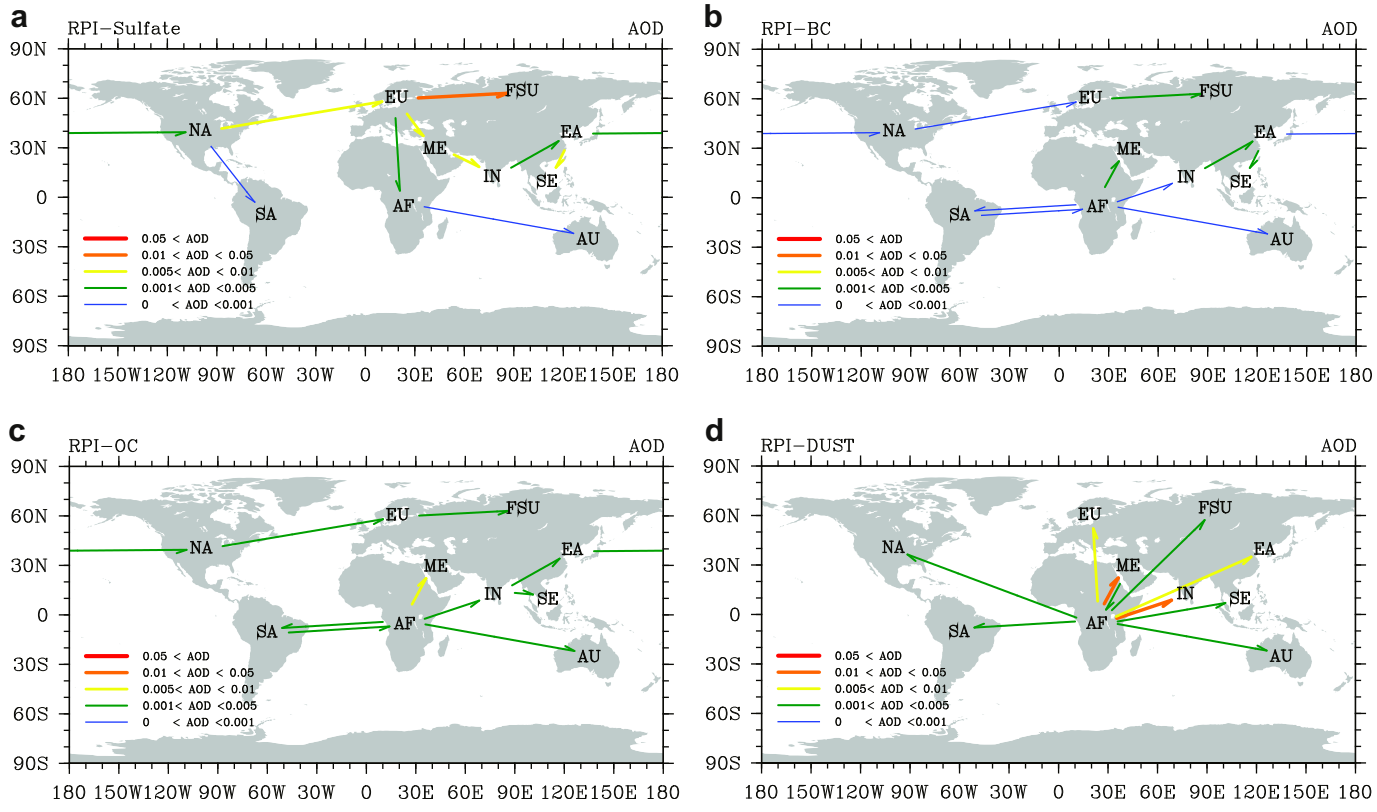


**Fig. 6.** Same as Fig. 5, but for the aerosol optical depth (AOD).

the ME (AF) carbonaceous aerosols (BC + OM) have the largest foreign influence on SAC (AOD) over IN. NA, SA, FSU, AU and ME receptors all have identical RPI for both AOD and SAC carbonaceous aerosols. Therefore, the dominant factor determining inter-continental influence patterns (based on RPI) is emission for dust aerosols, but is a combination of emission and transport efficiencies for other aerosol species.

## 5. Conclusions

Concerns are growing about the influence of inter-continental transport of air pollution, however a quantitative understanding of the contribution of foreign emissions to air quality is lacking. Here, we examine the source-receptor relationships between 10 continental regions for surface aerosol concentrations (SAC) and aerosol optical depths (AOD). We use the global chemical transport model MOZART-2 with both gas-phase and aerosol species, anthropogenic emissions for 2000 and meteorology for the period 1997–2003, to quantify the SAC of fine aerosols (diameters less than 2.5 μm (PM2.5)) and the AOD resulting from aerosols contributed by both emissions within the region and by inter-continental transport. We tag emissions of aerosol precursors and aerosol species from the continental source regions to track aerosol transport. We evaluate our model results by comparing simulated aerosol concentrations with observations from networks around the world. In general, the simulated aerosol concentrations agree within a factor of 2 with observations and capture the seasonal variation of aerosol concentrations in many parts of the world. An extensive model evaluation is presented in part two of the auxiliary material.

For each continental region, we establish source-receptor relationships in terms of area-weighted SAC and AOD resulting from domestic and inter-continental transport of sulfate, black carbon (BC), organic mass (OM) and fine dust aerosols. However, when interpreting these results it's important to realize that using large spatially averaged concentrations may mask sub-regional variability in the foreign contributions. The annual average fine aerosol concentrations (PM2.5) are largest in AF (26 $\mu g\,m^{-3}$), ME (25 $\mu g\,m^{-3}$), EA (18 $\mu g\,m^{-3}$), and IN (16 $\mu g\,m^{-3}$) due to large dust emissions (from AF, ME and EA) as well as large $SO_2$, and carbonaceous aerosols emissions (from EA, IN and AF), and are relatively small in other regions ($<8\ \mu g\,m^{-3}$). More than 80% of the SAC in AF, AU, EA, SA and NA occur as a result of emissions from domestic sources. Conversely, more than 40% of the SAC in SE, IN and the ME are transported from foreign regions.

The total AOD in each receptor due to all sulfate, carbonaceous and fine dust aerosols ranges from 0.04 (over AU) to 0.16 (over EA). For most receptors, background aerosols contribute a larger fraction of total aerosols to AOD than SAC, reflecting the free tropospheric maximum in inter-continental transport. For the FSU, ME and SE regions, background AOD is larger than domestic AOD. Sulfate and OM aerosols play dominant roles ($\sim$60%) in total AOD. Unlike SAC where fine dust is the major component for background aerosols, sulfate is the dominant contributor to background AOD in most receptor regions except IN (where dust dominates background AOD) and AU (where OM dominates background AOD).

Inter-continental transport of foreign aerosols dominates most receptors' background SAC and AOD. In order to highlight key source-receptor relationships and highlight the region from which emissions have the largest impact on a receptor's air quality (or solar radiation), we name this source region the Region of Primary Influence (RPI). Focusing on RPI will allow policymakers to identify key S–R influence patterns when considering possible future environmental agreements. We find that for each aerosol species, a receptor region usually has identical RPIs for SAC and AOD, particularly for dust, sulfate and BC aerosols. This indicates that reducing aerosol sources in RPI will simultaneously improve both surface air quality and visibility over the receptor region. For dust aerosols, AF is the RPI for all receptors for both SAC and AOD. For all non-dust species (i.e., sulfate, BC and OM), each receptor usually has only one or at most two RPIs for both SAC and AOD for different aerosol species. The following source-receptor pairs describe the key influence patterns for inter-continental transport of non-dust aerosols: EA → NA (i.e., EA is the RPI for NA for both SAC and AOD for all sulfate, BC and OM aerosols), (NA or AF) → **SA** (i.e., for each non-dust aerosol species, either NA or AF is SA SAC (or AOD) RPI), (NA or ME) → **EU**, EU → **FSU**, (EU or SA) → **AF**, (ME or AF) → **IN**, (IN or FSU) → **EA**, (EA or IN) → **SE**, AF → **AU**, and (EU or AF) → **ME**.

Unlike other aerosols, black carbon is not only an important component of PM2.5, but also strongly absorbs solar radiation (the single scattering albedo for black carbon is approximately 0.2–0.3) and hence contributes to both regional warming and dimming over a receptor region. The RPIs for BC in most receptors, including NA, SA, FSU, EA, SE, AU and ME, are identical for SAC and AOD. Therefore, the reduction of BC emissions from the RPI will not only improve the receptor's air quality and visibility, but may also reduce the warming effect of BC on the global atmosphere. International efforts which strengthen bilateral cooperation between receptor regions and their RPI to reduce black carbon emissions have the potential to simultaneously address the problems of air quality, regional dimming and potentially global warming as well (Levy et al., 2008). These types of agreements could be a first step in a global treaty to mitigate black carbon emissions.

## Acknowledgements

We thank Tami Bond for the black and organic carbon emission inventories, Huiyan Yang for sharing her dust code and Peter Hess for providing the MOZART-2 evaluation package. We thank Hajime Akimoto for providing observations from the EANET network, William Cooke for sharing BC and OC observational data, and Natalie Mahowald and Joseph Prospero for providing the dust observation data. We thank the Geophysical Fluid Dynamics Laboratory for computational resources. We are pleased to acknowledge funding from the Science, Technology and Environmental Policy (STEP) program at the Woodrow Wilson School of Public and International Affairs at Princeton University as well as funding from a NASA New Investigator Program grant to D. Mauzerall.

## Appendix. Supplementary data

Supplementary data associated with this article can be found, in the online version, at doi:doi:10.1016/j.atmosenv.2009.03.054.

## References

Benkovitz, C.M., Berkowitz, C.M., Easter, R.C., Nemesure, S., Wagener, R., Schwartz, S.E., 1994. Sulfate over the north-atlantic and adjacent continental regions – evaluation for October and November 1986 using a 3-dimensional model-driven by observation-derived meteorology. J. Geophys. Res. Atmos. 99, 20725–20756.

Benkovitz, C.M., Scholtz, M.T., Pacyna, J., Tarrason, L., Dignon, J., Voldner, E.C., Spiro, P.A., Logan, J.A., Graedel, T.E., 1996. Global gridded inventories of anthropogenic emissions of sulfur and nitrogen. J. Geophys. Res. Atmos. 101, 29239–29253.

Bond, T.C., Streets, D.G., Yarber, K.F., Nelson, S.M., Woo, J.H., Klimont, Z., 2004. A technology-based global inventory of black and organic carbon emissions from combustion. J. Geophys. Res. Atmos. 109, D14203. doi:10.1029/2003JD003697.

Brasseur, G.P., Orlando, J.J., Tyndall, G.S., National Center for Atmospheric Research (U.S.), 1999. Atmospheric Chemistry and Global Change, Topics in Environmental Chemistry. Oxford University Press, New York, xviii, 654 pp.

Cabada, J.C., Pandis, S.N., Robinson, A.L., 2002. Sources of atmospheric carbonaceous particulate matter in Pittsburgh, Pennsylvania. J. Air Waste Manag. Assoc. 52, 732–741.

Chin, M., Ginoux, P., Kinne, S., Torres, O., Holben, B.N., Duncan, B.N., Martin, R.V., Logan, J.A., Higurashi, A., Nakajima, T., 2002. Tropospheric aerosol optical thickness from the GOCART model and comparisons with satellite and sun photometer measurements. J. Atmos. Sci. 59, 461–483.

Chin, M., Diehl, T., Ginoux, P., Malm, W., 2007. Intercontinental transport of pollution and dust aerosols: implications for regional air quality. Atmos. Chem. Phys. 7, 5501–5517.

Cooke, W.F., Wilson, J.J.N., 1996. A global black carbon aerosol model. J. Geophys. Res. Atmos. 101, 19395–19409.

Cooke, W.F., Liousse, C., Cachier, H., Feichter, J., 1999. Construction of a 1 degrees × 1 degrees fossil fuel emission data set for carbonaceous aerosol and implementation and radiative impact in the echam4 model. J. Geophys. Res. Atmos. 104, 22137–22162.

Cooke, W.F., Ramaswamy, V., Kasibhatla, P., 2002. A general circulation model study of the global carbonaceous aerosol distribution. J. Geophys. Res. Atmos. 107 (D16), 4279. doi:10.1029/2001JD001274.

d'Almeida, G.A., Koepke, P., Shettle, E.P., 1991. Atmospheric Aerosols: Global Climatology and Radiative Characteristics. Deepak Publishing.

Davidson, C.I., Phalen, R.F., Solomon, P.A., 2005. Airborne particulate matter and human health: a review. Aerosol Sci. Technol. 39, 737–749.

Dentener, F., Stevenson, D., Cofala, J., Mechler, R., Amann, M., Bergamaschi, P., Raes, F., Derwent, R., 2005. The impact of air pollutant and methane emission controls on tropospheric ozone and radiative forcing: CTM calculations for the period 1990–2030. Atmos. Chem. Phys. 5, 1731–1755.

Dentener, F., Stevenson, D., Ellingsen, K., van Noije, T., Schultz, M., Amann, M., Atherton, C., Bell, N., Bergmann, D., Bey, I., Bouwman, L., Butler, T., Cofala, J., Collins, B., Drevet, J., Doherty, R., Eickhout, B., Eskes, H., Fiore, A., Gauss, M., Hauglustaine, D., Horowitz, L., Isaksen, I.S.A., Josse, B., Lawrence, M., Krol, M., Lamarque, J.F., Montanaro, V., Muller, J.F., Peuch, V.H., Pitari, G., Pyle, J., Rast, S., Rodriguez, J., Sanderson, M., Savage, N.H., Shindell, D., Strahan, S., Szopa, S., Sudo, K., Van Dingenen, R., Wild, O., Zeng, G., 2006. The global atmospheric environment for the next generation. Environ. Sci. Technol. 40, 3586–3594.

Derwent, R., Stevenson, D., Collins, W., Johnson, C., 2004. Intercontinental transport and the origins of the ozone observed at surface sites in Europe. Atmos. Environ. 38, 1891–1901.

Feichter, J., Kjellstrom, E., Rodhe, H., Dentener, F., Lelieveld, J., Roelofs, G.J., 1996. Simulation of the tropospheric sulfur cycle in a global climate model. Atmos. Environ. 30, 1693–1707.

Fiore, A.M., Dentener, F.J., Wild, O., Cuvelier, C., Schultz, M.G., Hess, P., Textor, C., Schulz, M., Doherty, R.M., Horowitz, L.W., MacKenzie, I.A., Sanderson, M.G., Shindell, D.T., Stevenson, D.S., Szopa, S., Van Dingenen, R., Zeng, G., Atherton, C., Bergmann, D., Bey, I., Carmichael, G., Collins, W.J., Duncan, B.N., Faluvegi, G., Folberth, G., Gauss, M., Gong, S., Hauglustaine, D., Holloway, T., Isaksen, I.S.A., Jacob, D.J., Jonson, J.E., Kaminski, J.W., Keating, T.J., Lupu, A., Marmer, E., Montanaro, V., Park, R.J., Pitari, G., Pringle, K.J., Pyle, J.A., Schroeder, S., Vivanco, M.G., Wind, P., Wojcik, G., Wu, S., Zuber, A., 2009. Multimodel estimates of intercontinental source-receptor relationships for ozone pollution. J. Geophys. Res. Atmos. 114, D04301. doi:10.1029/2008JD010816.

Ginoux, P., Chin, M., Tegen, I., Prospero, J.M., Holben, B., Dubovik, O., Lin, S.J., 2001. Sources and distributions of dust aerosols simulated with the gocart model. J. Geophys. Res. Atmos. 106, 20255–20273.

Ginoux, P., Horowitz, L.W., Ramaswamy, V., Geogdzhayev, I.V., Holben, B.N., Stenchikov, G., Tie, X., 2006. Evaluation of aerosol distribution and optical depth in the geophysical fluid dynamics laboratory coupled model CM2.1 for present climate. J. Geophys. Res. Atmos. 111, D22210. doi:10.1029/2005JD006707.

Giorgi, F., 1986. A particle dry-deposition parameterization scheme for use in tracer transport models. J. Geophys. Res. Atmos. 91, 9794–9806.

Grennfelt, P., Hov, O., 2005. Regional air pollution at a turning point. Ambio 34, 2–10.

Hadley, O.L., Ramanathan, V., Carmichael, G.R., Tang, Y., Corrigan, C.E., Roberts, G.C., Mauger, G.S., 2007. Trans-Pacific transport of black carbon and fine aerosols (d < 2.5 μm) into North America. J. Geophys. Res. Atmos. 112, D05309. doi:10.1029/2006JD007632.

Haywood, J.M., Ramaswamy, V., 1998. Global sensitivity studies of the direct radiative forcing due to anthropogenic sulfate and black carbon aerosols. J. Geophys. Res. Atmos. 103, 6043–6058.

Heald, C.L., Jacob, D.J., Park, R.J., Russell, L.M., Huebert, B.J., Seinfeld, J.H., Liao, H., Weber, R.J., 2005. A large organic aerosol source in the free troposphere missing from current models. Geophys. Res. Lett. 32, L18809. doi:10.1029/2005GL02383.

Heald, C.L., Jacob, D.J., Park, R.J., Alexander, B., Fairlie, T.D., Yantosca, R.M., Chu, D.A., 2006. Transpacific transport of Asian anthropogenic aerosols and its impact on surface air quality in the united states. J. Geophys. Res. Atmos. 111, D14310. doi:10.1029/2005JD006847.

Heald, C.L., Henze, D.K., Horowitz, L.W., Feddema, J., Lamarque, J.F., Guenther, A., Hess, P.G., Vitt, F., Seinfeld, J.H., Goldstein, A.H., Fung, I., 2008. Predicted change in global secondary organic aerosol concentrations in response to future climate, emissions, and land use change. J. Geophys. Res. Atmos. 113, D05211. doi:10.1029/2007JD009092.

Henze, D.K., Seinfeld, J.H., Ng, N.L., Kroll, J.H., Fu, T.M., Jacob, D.J., Heald, C.L., 2008. Global modeling of secondary organic aerosol formation from aromatic hydrocarbons: High- vs. Low-yield pathways. Atmos. Chem. Phys. 8, 2405–2420.

Horowitz, L.W., Walters, S., Mauzerall, D.L., Emmons, L.K., Rasch, P.J., Granier, C., Tie, X.X., Lamarque, J.F., Schultz, M.G., Tyndall, G.S., Orlando, J.J., Brasseur, G.P., 2003. A global simulation of tropospheric ozone and related tracers: description and evaluation of MOZART, version 2. J. Geophys. Res. Atmos. 108 (D24), 4784. doi:10.1029/2002JD002853.

Horowitz, L.W., 2006. Past, present, and future concentrations of tropospheric ozone and aerosols: methodology, ozone evaluation, and sensitivity to aerosol wet removal. J. Geophys. Res. Atmos. 111, D22211. doi:10.1029/2005JD006937.

Jacob, D.J., Crawford, J.H., Kleb, M.M., Connors, V.S., Bendura, R.J., Raper, J.L., Sachse, G.W., Gille, J.C., Emmons, L., Heald, C.L., 2003. Transport and chemical evolution over the Pacific (TRACE-P) aircraft mission: design, execution, and first results. J. Geophys. Res. Atmos. 108, 1–19.

Jaffe, D., McKendry, I., Anderson, T., Price, H., 2003. Six 'new' episodes of trans-pacific transport of air pollutants. Atmos. Environ. 37, 391–404.

Koch, D., Bond, T.C., Streets, D., Unger, N., 2007a. Linking future aerosol radiative forcing to shifts in source activities. Geophys. Res. Lett. 34, L05821. doi:10.1029/2006GL028360.

Koch, D., Bond, T.C., Streets, D., Unger, N., van der Werf, G.R., 2007b. Global impacts of aerosols from particular source regions and sectors. J. Geophys. Res. Atmos. 112, D02205. doi:10.1029/2005JD007024.

Levy, H., Schwarzkopf, M.D., Horowitz, L.W., Ramaswamy, V., Findell, K., 2008. Strong sensitivity of late 21st Century climate to projected changes in short-lived air pollutants. J. Geophys. Res. Atmos. 113, D06102. doi:10.1029/2007JD009176.

Liu, J.F., Mauzerall, D.L., 2005. Estimating the average time for inter-continental transport of air pollutants. Geophys. Res. Lett. 32, L11814. doi:10.1029/2005GL022619.

Liu, J.F., Mauzerall, D.L., Horowitz, L.W., 2005. Analysis of seasonal and interannual variability in transpacific transport. J. Geophys. Res. Atmos. 110, D04302. doi:10.1029/2004JD005207.

Liu, J.F., Mauzerall, D.L., 2007. Potential influence of inter-continental transport of sulfate aerosols on air quality. Environ. Res. Lett. (2) 045029. doi:10.1088/1748-9326/2/4/045029.

Liu, J.F., Mauzerall, D.L., Horowitz, L.W., 2008. Source-receptor relationships of trans-pacific transport of East Asian sulfate. Atmos. Chem. Phys. 8, 5537–5561.

Liu, J.F., Mauzerall, D.L., Horowitz, L.W. Evaluating inter-continental transport of fine aerosols: (2) global health impact, submitted for publication.

Mahowald, N.M., Muhs, D.R., Levis, S., Rasch, P.J., Yoshioka, M., Zender, C.S., Luo, C., 2006. Change in atmospheric mineral aerosols in response to climate: last glacial period, preindustrial, modern, and doubled carbon dioxide climates. J. Geophys. Res. Atmos. 111, D10202. doi:10.1029/2005JD006653.

Malm, W.C., Sisler, J.F., Huffman, D., Eldred, R.A., Cahill, T.A., 1994. Spatial and seasonal trends in particle concentration and optical extinction in the United-States. J. Geophys. Res. Atmos. 99, 1347–1370.

Marticorena, B., Bergametti, G., 1995. Modeling the atmospheric dust cycle.1. Design of a soil-derived dust emission scheme. J. Geophys. Res. Atmos. 100, 16415–16430.

Martin, L.R., Damschen, D.E., 1981. Aqueous oxidation of sulfur-dioxide by hydrogen-peroxide at low PH. Atmos. Environ. 15, 1615–1621.

Ming, Y., Ramaswamy, V., Ginoux, P.A., Horowitz, L.H., 2005. Direct radiative forcing of anthropogenic organic aerosol. J. Geophys. Res. Atmos. 110, D20208. doi:10.1029/2004JD005573.

Muller, J.F., 1992. Geographical-distribution and seasonal-variation of surface emissions and deposition velocities of atmospheric trace gases. J. Geophys. Res. Atmos. 97, 3787–3804.

Muller, J.F., Brasseur, G., 1995. Images – a 3-dimensional chemical-transport model of the global troposphere. J. Geophys. Res. Atmos. 100, 16445–16490.

Park, R.J., Jacob, D.J., Chin, M., Martin, R.V., 2003. Sources of carbonaceous aerosols over the united states and implications for natural visibility. J. Geophys. Res. Atmos. 108 (D12), 4355. doi:10.1029/2002JD003190.

Park, R.J., Jacob, D.J., Field, B.D., Yantosca, R.M., Chin, M., 2004. Natural and trans-boundary pollution influences on sulfate-nitrate-ammonium aerosols in the united states: implications for policy. J. Geophys. Res. Atmos. 109, D15204. doi:10.1029/2003JD004473.

Prospero, J.M., 1996. The atmospheric transport of particles to the ocean, in particle flux in the ocean. In: Ittekkot, v., Schäfer, p., Honjo, s., J. Depetris, p. (Eds.), Scope, vol. 57, pp. 19–52.

Saikawa, E., Naik, V., Horowitz, L.W., Liu, J., Mauzerall, D.L., 2009. Present and potential future contributions of sulfate, black and organic carbon aerosols from China to global air quality, premature mortality and radiative forcing. Atmos. Environ. 43 (17), 2814–2822.

Sanderson, M.G., Dentener, F.J., Fiore, A.M., Cuvelier, C., Keating, T.J., Zuber, A., Atherton, C.S., Bergmann, D.J., Diehl, T., Doherty, R.M., Duncan, B.N., Hess, P., Horowitz, L.W., Jacob, D.J., Jonson, J.E., Kaminski, J.W., Lupu, A., MacKenzie, I.A., Mancini, E., Marmer, E., Park, R., Pitari, G., Prather, M.J., Pringle, K.J., Schroeder, S., Schultz, M.G., Shindell, D.T., Szopa, S., Wild, O., Wind, P., 2008. A multi-model study of the hemispheric transport and deposition of oxidized nitrogen. Geophys. Res. Lett. 35, L17815. doi:10.1029/2008GL035389.

Seinfeld, J.H., Pandis, S.N., 1998. Atmospheric Chemistry and Physics: From Air Pollution to Climate Change. Wiley, New York, xxvii, 1326 pp.

Shindell, D.T., Chin, M., Dentener, F., Doherty, R.M., Faluvegi, G., Fiore, A.M., Hess, P., Koch, D.M., MacKenzie, I.A., Sanderson, M.G., Schultz, M.G., Schulz, M., Stevenson, D.S., Teich, H., Textor, C., Wild, O., Bergmann, D.J., Bey, I., Bian, H., Cuvelier, C., Duncan, B.N., Folberth, G., Horowitz, L.W., Jonson, J., Kaminski, J.W., Marmer, E., Park, R., Pringle, K.J., Schroeder, S., Szopa, S., Takemura, T., Zeng, G., Keating, T.J., Zuber, A., 2008. A multi-model assessment of pollution transport to the Arctic. Atmos. Chem. Phys. 8, 5353–5372.

Stevenson, D.S., Dentener, F.J., Schultz, M.G., Ellingsen, K., van Noije, T.P.C., Wild, O., Zeng, G., Amann, M., Atherton, C.S., Bell, N., Bergmann, D.J., Bey, I., Butler, T.,

Cofala, J., Collins, W.J., Derwent, R.G., Doherty, R.M., Drevet, J., Eskes, H.J., Fiore, A.M., Gauss, M., Hauglustaine, D.A., Horowitz, L.W., Isaksen, I.S.A., Krol, M.C., Lamarque, J.F., Lawrence, M.G., Montanaro, V., Muller, J.F., Pitari, G., Prather, M.J., Pyle, J.A., Rast, S., Rodriguez, J.M., Sanderson, M.G., Savage, N.H., Shindell, D.T., Strahan, S.E., Sudo, K., Szopa, S., 2006. Multi-model ensemble simulations of present-day and near-future tropospheric ozone. J. Geophys. Res. Atmos. 111. doi:10.1029/2005JD006338.

TF-HTAP, 2007. Hemispheric Transport of Air Pollution 2007, United Nations Economic Commission for Europe, New York and Geneva. In: Air Pollution Studies, No. 16. http://www.htap.org.

Tie, X., Brasseur, G., Emmons, L., Horowitz, L., Kinnison, D., 2001. Effects of aerosols on tropospheric oxidants: a global model study. J. Geophys. Res. Atmos. 106, 22931–22964.

Tie, X.X., Madronich, S., Walters, S., Edwards, D.P., Ginoux, P., Mahowald, N., Zhang, R.Y., Lou, C., Brasseur, G., 2005. Assessment of the global impact of aerosols on tropospheric oxidants. J. Geophys. Res. Atmos. 110, D03204. doi:10.1029/2004JD005359.

van der Werf, G.R., Randerson, J.T., Collatz, G.J., Giglio, L., 2003. Carbon emissions from fires in tropical and subtropical ecosystems. Glob. Change Biol. 9, 547–562.

van der Werf, G.R., Randerson, J.T., Collatz, G.J., Giglio, L., Kasibhatla, P.S., Arellano, A.F., Olsen, S.C., Kasischke, E.S., 2004. Continental-scale partitioning of fire emissions during the 1997 to 2001 El Nino/La Nina period. Science 303, 73–76.

Zender, C.S., Bian, H.S., Newman, D., 2003. Mineral dust entrainment and deposition (DEAD) model: description and 1990s dust climatology. J. Geophys. Res. Atmos. 108 (D14), 4416. doi:10.1029/2002JD002775.